Development of Sn-Li alloys for application in Fusion Nuclear Reactors

Miguel Fraústo de Brito Costa
miguel.brito.costa@tecnico.ulisboa.pt

Instituto Superior Técnico, Lisbon, Portugal

October 2018

Abstract

Nuclear Fusion offers the possibility of a large-scale energy source. One of the main challenges to overcome in the path to harnessing fusion power is the choice of materials for plasma facing components. Sn-Li alloys have been shown to be a possible candidate. This work proposes the mechanical alloying route to produce Sn-Li alloys from 5at% Li to 25at% Li avoiding the formation of high temperature Li_xSn_y intermetallic compounds, segregation and larger scale microstructures characteristic of the liquid route.

Ball milling experiments were conducted on pure Sn powders, both under air and argon atmosphere, to obtain references for milling in the Sn-Li system. Sn-Li mechanical alloying and cold pressing were carried out under argon starting from pure gas atomized Sn powders and small ribbon cut Li bits. The produced powders and pellets were studied to assess the morphological (SEM/EDS), compositional (IBA) and phase (DRX and DSC) evolution with milling conditions.

The morphology of milled particles evolves with milling time starting as cold welded, rugose particles, then towards spherical or faceted, smooth particles and finally to thin large discs. Cold-welding is the predominant mechanism observed up to 24h of milling. A dispersion of Li-rich particles is observed for all compositions. Due to the dry conditions used, the yield of the technique is limited due to excessive adhesion of cold-welded milled materials to the vial wall (<20% after 24h effective milling time).

IBA analysis identified that small deviations from the designed Li bulk concentrations were observed: Sn-25Li had a concentration of 17,0 (±4,4)at% after 2h and 22,3 (±4,9)at% after 12h of milling, Sn-15Li had a concentration of 16,5 (±14,9)at% after 2h and 11,0 (±1,5)at% after 12h of milling and Sn-5Li has a concentration of 4,2 (±0,3)at% after 2h and 3,8 (±0,6)at% after 12h of milling. The large standard deviations observed in the higher Li atomic percentage alloys (Sn-25Li and Sn-15Li) are due to inhomogeneity of the processed powders.

The main phases and phase transformations identified with XRD and DSC are the $L \longrightarrow Sn + Li_2Sn_5$ eutectic, pure Sn, Li_2Sn_5 and LiSn intermetallic. The presence of higher Li content intermetallic compounds could not be confirmed.

Keywords: Mechanical Alloying; Sn Ball Milling; Sn-Li alloys; Nuclear Fusion Blanket Materials.

1. Introduction

Compatibility between plasma and the first wall material is one of the main challenges in designing a nuclear fusion reactor. The parts exposed to the plasma are designed to be resistant to high heat and neutron fluxes, thermal conductive, resistant to physical and chemical erosion, and of low tritium retention. R&D on plasma surface interactions (PSI) and plasma facing components (PFCs) with a liquid surface has included liquid gallium, tin, lithium and Sn-Li alloys [1].

Sn-Li alloys production by casting has proved to be difficult due to segregation of Li to the surface of the melt. Special care must be taken to avoid separation of both elements [2], [3]. In this work, a solid-state route for production of Sn-Li alloys by mechanical alloying is proposed. Mechanical alloying (MA) is a solid-state powder processing technique that involves repeated cold welding, fracturing, and rewelding of powder particles in a high-energy ball mill induced by trapping of powders between the milling media and the vial. Alloying occurs between the desired elemental powders and, ideally, a homogeneous alloy is obtained at the end of processing [4].

2. State-of-the-Art

1.1. Liquid Metal Plasma Facing Components

For the next step devices, e.g. DEMO, or a future fusion reactor, the limits on power-exhaust and lifetime of components are strict. Radiation effects and neutron embrittlement limit the actively cooled W components in DEMO to about 3–5 MW/m^{-2}. Erosion of the first wall requires significant reinforcement of armour thickness or short exchange intervals, while high-power

transients need strong mitigation efficiency to prevent PFC's damage. Liquid metals have long been suggested to improve lifetime and power-exhaust issues due to their self-healing, self-replenishing surfaces with no susceptibility to neutron damage [5].

Apart from sputter-erosion, as known for solid PFCs, evaporation rates must be considered for use of liquid metal PFC's. Depending on the impurity and its atomic number (Z), the influence on the plasma can be quite different, ranging from fuel dilution of the fusion plasma (low-Z) to radiative collapse (high-Z). The evaporative limit is usually compared with reference to the incoming plasma flux ($\sim 10^{24}$ m^{-2} s^{-1}) [5].

Requirements for PFC's materials include good thermal and electrical conductivity, resistance to thermal shock and erosion processes, low tritium retention, low activation and short-life products under neutron irradiation, low probability of ending up in the core plasma and, if ending up is unavoidable, low Z.

The main candidate elements for liquid metal surfaces for fusion reactor are Ga, Li and Sn: the three elements have intrinsic good thermal and electric properties, resistance to thermal shock and erosion. However, tritium retention, activation by neutron bombardment and probability of ending up in the core plasma, mainly due to evaporation induced by high temperatures or sputtering, must be addressed.

Li is the most attractive material for LM walls and the most extensively researched. Because of its low Z, the radiation loss is not enhanced when it stays in a core plasma and fresh lithium surfaces absorbs impurities so that the lithium wall coverage leads to significant improvement of plasma performance [6].

However, two main issues are found for use of pure Li as coating for the first wall: Li has a high vapour pressure and evaporation rate increases exponentially above its melting temperature. A maximum temperature of 490ºC is predicted for Li surfaces in the reactor chamber, which can be easily reached in fusion reactor conditions. Li high affinity for H isotopes also makes reliable tritium removal difficult.

2.2. Sn-Li Alloys Properties

Figure 1 is a schematic illustration of the Sn–Li phase diagram, which shows several Li–Sn compounds (such as Li_2Sn_5, LiSn, Li_5Sn_2, Li_7Sn_3, $Li_{13}Sn_5$ and $Li_{22}Sn_5$) that exhibit melting temperatures of 485ºC – 783 ºC.

Sn-Li alloys display beneficial properties, which also qualify them as suitable candidates for liquid surfaces in fusion reactor. The evaporative flux of the 20Sn-Li alloy is at least three orders of magnitude lower than pure Li. This leads to a wall temperature limit of about 700°C for this alloy compared to the 490°C for pure Li.

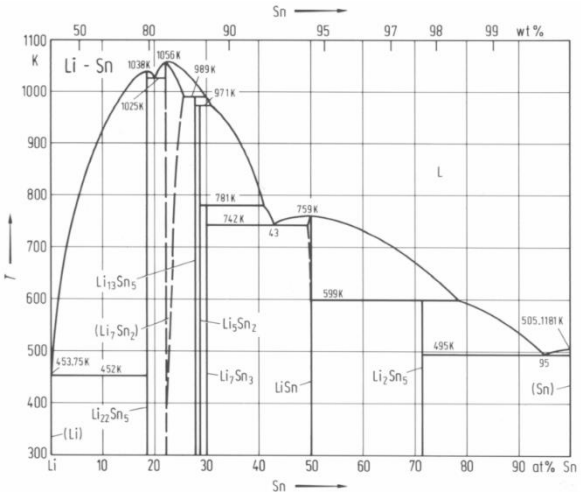

Figure 1 – Sn-Li binary phase diagram (adapted from [26]*).*

Also, liquid Sn-Li alloys has been shown to possess low solubility of deuterium. As such, a high-recycling regime is expected [7], [8]. Vapour from evaporated liquid 20Sn-Li is dominated by the lithium component [8]. The reason for that is the surface segregation of Li atoms in the alloy, producing a surface layer enriched in Li when exposed to the plasma while keeping a low vapour pressure and very low H retention characteristic of Sn [9].

2.3. Sn-Li Alloys Production

Sn-Li alloys have been previously produced via liquid state route [2] by slowly adding liquid Li to an Sn molten bath, slowly increasing the content of Li to avoid formation of stable compounds due to Li segregation. Quick stirring was used to ensure good mixing of both elements. To homogenize the liquid alloy, very long stirring (up to three days) and temperatures in the interval 400-500ºC were needed. The authors claim that two phases were present in the final microstructure, Sn and eutectic Sn + Li_2Sn_5.

On a more recent study [3], Sn-Li alloys with contents of 20, 25 and 30 at% Li were produced by melting granules of Li and Sn. The best results were attained after homogeneously mixing the powders before melting to avoid Li segregation. Li depletion was observed due to Li oxidation due to oxygen present in the initial powders.

Mechanical alloying of Sn-Li powders has also been carried out [10], [11]. However, the objective of this study was to produce Li_xSn_y intermetallic compounds for application in the fuel cell area. In these experiments, stoichiometric amounts of Li and Sn were ball milled and then sintered in vacuum. LiSn, $Li_{13}Sn_5$, Li_7Sn_2 and $Li_{22}Sn_5$ intermetallic samples were produced and characterized. However, this work gives special attention to the Mossbauer spectroscopy characterization of the produced samples and little

information is present about the experimental procedure or the products obtained after processing.

3. Experimental Procedure

Small pieces of Li metal (99%, ~2mm, Sigma-Aldrich) and Sn atomised powders (99.7%, <45 µm, Makin Metal Powders (UK) Ltd) were used as starting materials.

Ball milling experiments of pure Sn with different speeds (150 and 300RPM), atmospheres (air and argon), milling balls size (6mm and 10mm) and up to 64h effective milling time were tested as reference for the Sn-Li system.

Alloys with 25, 15 and 5 Li at% were produced. Approximately 3g of elemental powders were milled in each batch. No process control agent (PCA) was used. The ball-to-powder ratio was kept at 10:1. Experiments were conducted on a Retsch PM100 planetary ball mill using a 50mL vial loaded with 6mm milling balls, both made of AISI 420C steel. Powders were milled for 2, 12 and 24 hour's effective milling time with 5 minutes pause time after every 10 minutes running time. Powder loading into the vial was carefully controlled inside a glove box (MBraun Unilab Plus) with dry Ar atmosphere (<0,1ppm H_2O / O_2). The vial was closed inside the glove box with an air tight security hatch to ensure inert atmosphere during processing and afterward. The vial was only opened again once back inside the glove box.

A JEOL field emission scanning electron microscope (FE-SEM) model JSM-7001F equipped with an Oxford Light Elements EDS Detector and a HITACHI model S-2400 with a Bruker Esprit 1.9, EDS Bruker SDD light element detector were used to observe the powder morphology and composition. Ion Beam Analysis (IBA) was conducted in the 2.5 MeV Van de Graaff accelerator of CTN/IST. XRD characterization was performed with a Phillips PW 1830 using Cu-Kα radiation (tension of 40kV and current 30mA). The diffractograms were obtained with a step of 0.04º and acquisition time of 8 seconds. Samples tested with XRD were covered in paraffin to prevent reaction with air during characterization. DSC thermal analysis for phase determination was performed with a TA instruments Q200 V24.4 DSC equipment with a maximum temperature of 350ºC with heating ramps of 10ºC/min under N_2 atmosphere.

4. Results

4.1. Pure Sn results

For both atmospheres tested, initially, the fine powders cold-weld together forming small cold-welded agglomerates. These particles evolve to become spherical, shell-like and lamellar particles. The main differences when using different atmospheres become noticeable between 4-8h of milling. When air atmosphere was used, a tin oxide film forms at the particles surface. This film breaks down with the ball media impacts during milling, dispersing the resulting oxide particles in the tin matrix. The dispersion of oxides effectively hardens the material, decreasing the fracture toughness and reducing the adhesion and cold-welding ability. In air, particles evolve to become lamellar particles and in later stages into flake-like particles, once cracking becomes the predominant mechanism, thus reducing the particle size. In Argon this effect does not occur, and particles keep increasing up to 12-16h of milling. After these effective milling times the particles' size seems to remain constant.

4.2. Sn-Li results

4.2.1. Morphological Analysis

The Sn-25Li alloy powders were observed at 2h, 12h and 24h of milling time (Figure 2). The cross-section of the powders was also observed for in depth microstructural analysis.

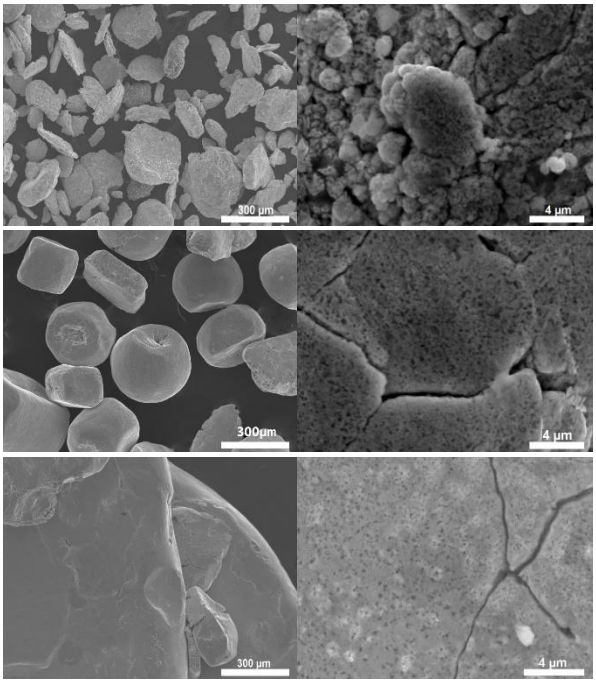

Figure 2 – Sn-25Li alloy SEM micrograph: a) and b) 2h milled, c) and d) 12h milled, e) and f) 24h milled.

After 24h milling time the samples take the form of thin large discs of cold-welded material. This is a frequent problem found when Li metal is used in mechanical alloying experiments. Previous research in systems such as Fe-Li [12]–[14], Cu-Li [13] and Si-Li [14] show that when the content of Li increases the difficulty of producing powders also increases due to excessive cold welding and adhesion to the milling media and vial [12]–[14]. The morphology of the powders of the Sn-25Li alloy indicates an evolution

with milling time, starting as lamellar, rugose particles (Figure 2a-b) and evolving to more faceted, smooth particles (Figure 2b-f).

At higher magnifications, both at the powder surfaces and powder cross-sections, a dimpled-like morphology is revealed with dark round spots distributed on a clearer grey matrix (Figure 2b/d/f). The dark round pattern is still observable in the cross-section of all the samples, thus showing it's not a surface phenomenon. Compositional analysis indicates that the darker zones have higher oxygen content than the grey zones. The dark colour and the presence of excess oxygen leads to believe these are Li rich zones while the grey matrix should have higher contents of Sn. A chemical reaction occurred near the dark particles of this dimpled-like morphology at the surface during exposure to air indicating a preferential reaction site with air, likely to enhanced reactivity of Li. The circular geometry of these dark particles and its homogeneous dispersion in the matrix leads to believe that these particles are the result of a nucleation burst of Li-rich intermetallic promoted by the extreme high mobility of Li in Sn at the processing temperature [15], [16].
Severe cracking at the surface of the powders are most likely resultant from the formation of Li_2Sn_5. Li_2Sn_5 has a density of 5,97g/cm^3 which corresponds to a 20% volume increase compared to the β-Sn matrix. As the intermetallic phase forms a volumetric expansion occurs. This expansion coupled with the fragile behaviour of the intermetallic phase [17] generates cracks in the particles. As milling proceeds the cracks are closed by the milling process as Sn ductile behaviour is predominant. Due to the high homologous temperature of the process creep may also contribute to closing of the cracks.

The powders milled for 12h are larger than those milled for 2h. After 24h most of the material is welded to the vial walls and the remaining free particles are very large (millimetre range), which indicates that up to 24h of milling the predominant mechanism is the cold welding of particles. The cracks at the surface indicate presence of fragile phases while the overall evolution of the milled particles indicates ductile behaviour. It was also observed that as the milling time increases, the amount of welded powders adhering to the vial walls also increases. This is also consistent with the ductile behaviour of the material being milled. It's likely that fragile phases form mainly at the powder's surface, but they are dispersed in a ductile matrix which dominates the overall mechanical behaviour of the particles being milled.

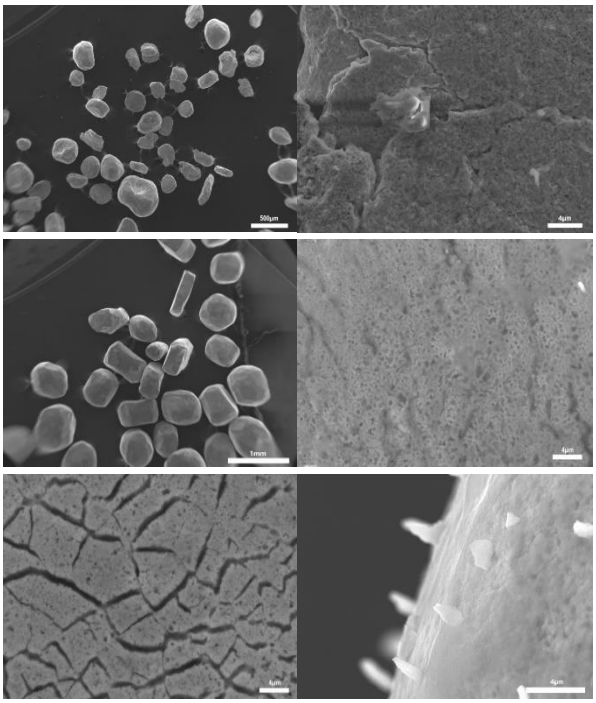

Figure 3 – Sn-Li alloys SEM micrographs: a) and b) Sn-15Li alloy 2h milled and c) and d) Sn-5Li alloy 2h milled.

For the two remaining alloys, Sn-15Li and Sn-5Li, only the powders milled for 2h were observed. The powders of the alloy Sn-15Li (Figure 3a-b) show significant differences when compared to the Sn-25Li powders (Figure 2a-b). The particles milled for 2h are rounder and less rugose than the more Li rich composition for the same milling time. The same dimpled-like morphology, with dark round spots was observed (Figure 3b). They appear to be approximately the same size as those found in the 25at% Li alloy (<250nm). However, the area covered by the dispersion of dark round particles is smaller, with some clearly preferential areas for the nucleation.

There is also considerably less cracking than in the previous alloy composition, while the discontinuities present seem to be mostly from cold welding, leading to believe that a smaller fraction of fragile phases is present. This was to be expected as the fragile phases formed during milling are most likely Sn-Li intermetallic compounds, which decrease in amount as the Li content decreases.

The particles of Sn-5Li alloy milled for 2h (Figure 3c-d) possess less surface rugosity than the other two alloys and after just 2h of milling they are faceted (very similar to the Sn-25Li alloy powders milled for 12h). The dimpled-like pattern was recognized covering a fraction of the surface area (Figure 3d-e). Small whiskers formed at the particle surface (Figure 3f). It's possible that the whiskers observed also form in the higher Li concentration alloys but could be masked by the remaining surface rugosity. EDS analysis was carried out on the whiskers, indicating oxygen as the

overwhelmingly major element (>95at%) indicating the whiskers are most likely Lithium oxide with unknown stoichiometry. Considering the geometry and composition of the whiskers, the following mechanism is proposed for its formation: as small columns of oxide grow outwards from the surface, the formation of oxide must occur at the interface between the particle and the whisker. As oxygen diffuses to the interface (gas phase transport) lithium diffuses from the inside of the particle (solid state diffusion rate controlling step). More Lithium oxide forms at the interface, continuously pushing the lithium oxide whisker already present further away from the particle surface, forming small columns as observed by SEM.

4.2.2. Compositional Analysis

An example of an EBS+RBS+NRA spectrum and the corresponding best fit line for a Sn-Li alloy sample is shown in Figure 4.

EBS+RBS yields are presented in linear scale (Figure 4a)) to provide better observation of the peaks of the elements detected. ERS+RBS+NRA yields are presented in logarithmic scale (Figure 4b)) for a better representation of the NRA yield segment.

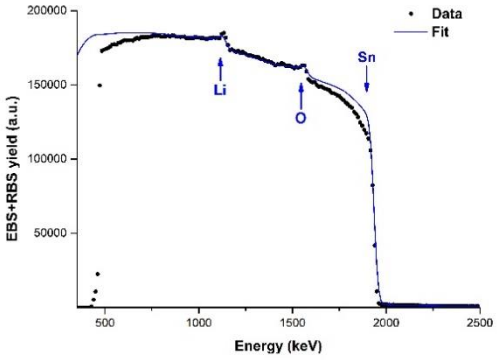

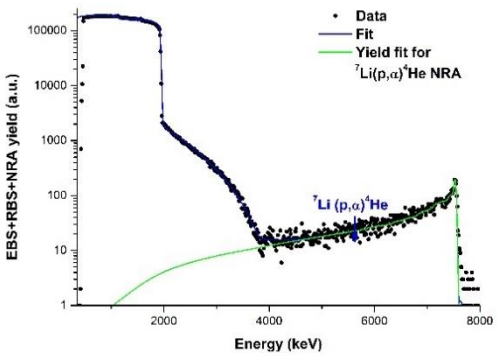

Figure 4 - ERS/RBS/NRA spectra of a Sn-25Li alloy, 2h milled sample point: a) EBS+RBS yield of sample milled, b) EBS+RBS+NRA yield of sample.

Table 1 - Sn-Li alloys samples calculated average concentration and respective standard deviation results according to best IBA fit.

Alloy	Surface		Bulk	
Sn-25Li	**Li at%**	**O at%**	**Li at%**	**O at%**
2h	47,3 (±2,5)	49,0 (±1,7)	17,0 (±4,4)	<0,5
12h	42,0 (±3,5)	25,0 (±0,0)	22,3 (±4,9)	<0,5
Sn-15Li				
2h	45,7 (±4,0)	45,0 (±5,0)	16,5 (±14,9)	<0,5
12h	46,3 (±1,5)	46,3 (±3,2)	11,0 (±1,5)	<0,5
Sn-5Li				
2h	42,3 (±7,5)	41,7 (±10,4)	4,2 (±0,3)	<0,5
12h	42,7 (±4,0)	47,33 (±6,8)	3,8 (±0,6)	<0,5

Analysis indicates inhomogeneities in the concentration of the analysed pellets. A common effect observed was a surface segregation of Li and a higher surface concentration of oxygen. The high oxygen content at the surface results from the exposure of the alloy pellets to air during sample loading in the IBA stage. Oxygen concentration decreases rapidly to a value below 0.5at% after a few hundred nanometres in all alloy compositions. All calculated IBA spectra and concentration profiles assume an in-depth oxygen concentration of 0.5at%. This value was considered as an upper limit for the bulk concentration of oxygen but it's likely that the real value for the concentration is lower than 0.5 at% (according to best fit of IBA results).

The average surface concentration and bulk concentration of the pellets of the 25Li-, 15Li- and Sn-5Li alloys can be seen in Figure 5. A typical concentration profile of the analysis performed on a Sn-5Li pellet up to a depth of 17-20µm is shown in Figure 5.

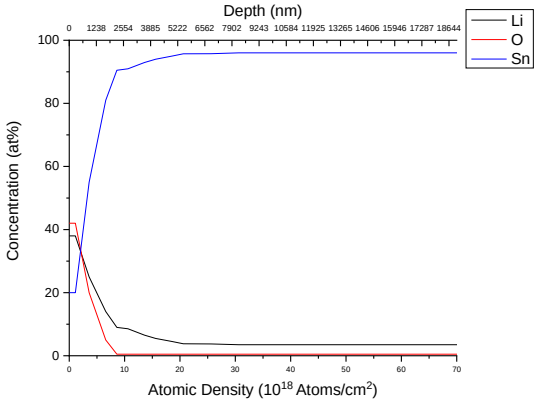

Figure 5 - Concentration profile of a Sn-5Li 12h milled sample. Y axis shows atomic concentration plotted vs atomic density (bottom X axis). Top X axis provides an approximation of the depth according to the atomic density of the alloy.

The concentration profile of all analysed points is very similar: the concentration of Li and oxygen steadily decreases and stabilize after a few microns while the Sn concentration changes accordingly. The Sn-25Li sample milled for 12h was the only sample with non-consistent results. For this composition, an increase in concentration of Li with depth increase is observed (~40 at% at surface vs ~50 at% after 3µm). This is followed by a decrease of Li concentration until the maximum depth analysed. There is also a significantly lower concentration of oxygen at the surface (25at%) compared with the surface concentrations observed for the remaining samples (<40at%). However, the concentration of oxygen does not decrease as steeply as the other samples analysed.

A small deviation from the designed Li bulk concentrations is observed: Sn-25Li has a concentration of 17,0 (±4,4)at% after 2h of milling and 22,3 (±4,9)at% after 12h of milling; Sn-15Li has a concentration of 16,5 (±14,9) at% after 2h of milling and 11,0 (±1,5) at% after 12h of milling and Sn-5Li has a concentration of 4,2 (±0,3) at% after 2h and 3,8 (±0,6) at% after 12h. The Sn-25Li alloy and Sn-15Li alloy seem to have an increase in the bulk Li concentration with an increase in milling time. After 2h of milling there were still large chunks of unmixed Li which could be seen with the naked eye. This shows that alloys with higher Li content take longer to homogenize. The Sn-5Li alloy apparently shows a different tendency: after 2h the bulk concentration of Li seems to be higher than after 12h. After 2h there was no longer any unmixed Li. The proceeding of the milling operation of the mixed powders could result in loss of Li to the walls. However, the difference in Li content could also be attributed to local inhomogeneity of the pellet or local loss of Li due to segregation towards the surface.

The large standard deviation of the Sn-15Li alloy milled for 2h is also a result of local inhomogeneity. It was observed that some points of the 25 and Sn-15Li alloys displayed Li content above the design composition (>27% in depth Li concentration) which indicates that in some cases full homogenization was not attained, which are evidenced by the calculated higher standard deviation for these alloys.

The segregation of Li to the surface is observed in all compositions. Li concentrations in the interval 35-50at% were calculated for the surface layers of all produced pellets. Two mechanisms are proposed to sustain the Li surface segregation: the first, considered the main mechanism, is the diffusion of Li from the bulk to the surface due to the chemical potential gradient induced by Li oxide formation at the surface. Random existing surface Li atoms react with atmospheric oxygen to form Li oxide. The arrival of fresh oxygen from the atmosphere induces oxide growth supported by fast Li diffusion from the bulk. Assuming a conservative approach with a room temperature diffusion coefficient of 10^{-10} m^2/s and 10 minutes exposure to air during sample preparation the diffusion length, $\sqrt{Dt}$, is 245 µm. In this work, the observed affected diffusion depth was <15µm for all points examined with IBA. Considering the value of $\sqrt{Dt}$, the results for Li surface segregation are acceptable. The second supplementary mechanism may be attributed to the difference in the surface energy of Li and Sn. Li has a lower surface energy than Sn [18]. As such, a reduction of surface energy is expected when Li concentration at the surface increases, promoting diffusion of the bulk Li towards the surface, even in the absence at the surface of oxygen [18]. The characterization of the surface without exposure to oxygen was impossible in the scope of this work and as such the contribution of each mechanism described above could not be assessed. The values of the concentration of each element at the sample surface lead to believe that the surface is composed of a mixture of oxides such as SnO, SnO_2, Li_2O and Li_2O_2.

4.2.3. Phase Analysis

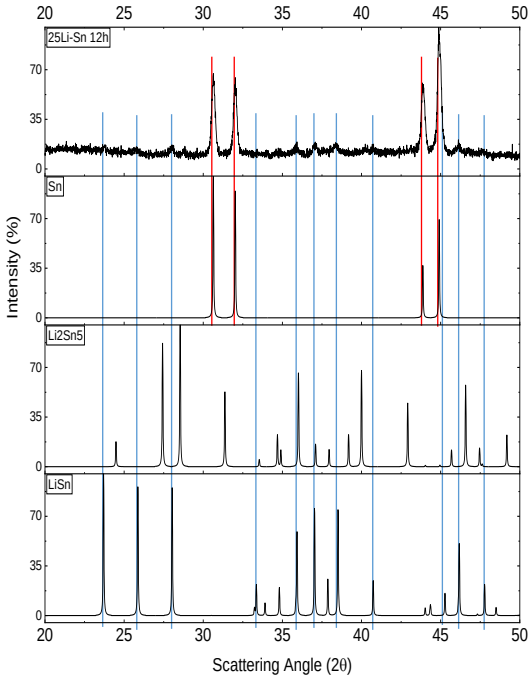

Figure 6 - XRD diffractogram of Sn-25Li alloy sample milled 12h. The peaks of two phases are represented in the diffractogram: β-Sn (red) and LiSn (blue).

Despite the low cross-section of Li detection in XRD analysis, the LiSn peaks can be clear distinguished in the diffractogram of a Sn-25Li 12h milled sample (Figure 6). However, the presence of LiSn could not be confirmed in the remaining analysis neither on the thermal analysis conducted with DSC. XRD were also carried out on the Sn-25Li alloy 2h milled. Only β-Sn peaks were detected in the obtained diffractograms.

A DSC thermal cycle, between 50 ºC - 250ºC, with a double heating cycle, was performed on all Sn-Li alloys produced. On the Sn-25Li alloy, an extra thermal cycle up to 340ºC was tested. Examples of the obtained DSC spectra are shown in Figure 7.

On the 1st heating cycle of the 50ºC – 250ºC test of the Sn-25Li alloy samples (both 2h and 12h milled), two endothermic transformations are observed: the eutectic transformation and pure Sn melting.

The eutectic decomposition is associated with an enthalpy of fusion of -8065 J/mol [19] while Sn has a enthalpy of fusion of -7179 J/mol [20]. Based on the peak integral and the enthalpy of fusion of both reactions it is concluded that more Sn is detected than eutectic mixture for both samples. Considering that the bulk composition of the alloy, 25Li, has a surplus of Li relative to the eutectic composition (~5%at Li), no detection of free β–Sn would be expected, only the β–Sn of the eutectic phase. This shows that there is a deviation from equilibrium resultant from sampling and material processing.

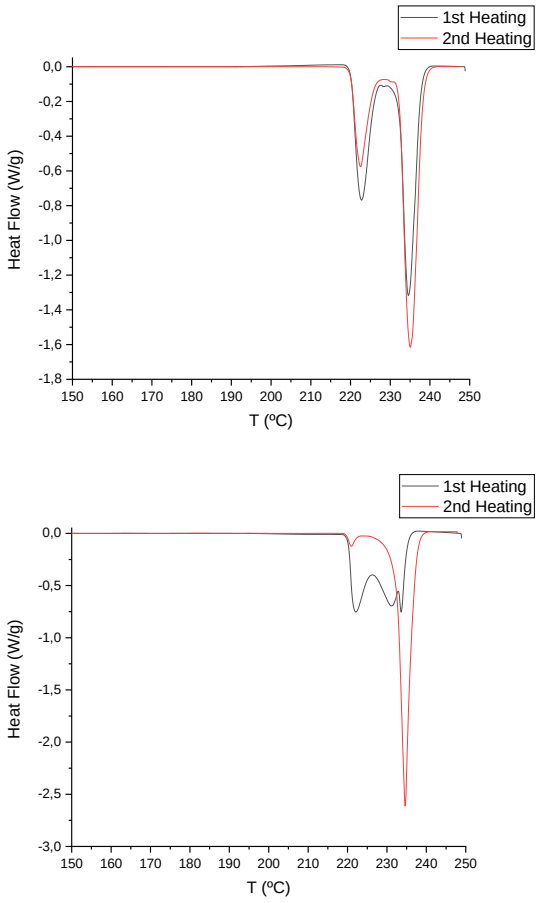

Figure 7 - DSC curves of Sn-Li alloys samples: a) Sn-25Li, 2h milled, two endothermic peaks and b) Sn-15Li, 12h milled, three endothermic peaks.

On the 2nd heating cycle of this analysis there are noticeable differences in both samples' thermal behaviour, indicating that a non-reversible phase transformation (within the tested temperature interval, 50ºC – 250ºC) took place after the 1st heating cycle: the general tendency observed was for a significant decrease in the eutectic transformation peak heat flow with an increase of that for Sn melting. This indicates that the amount of free β–Sn has increased after the first run in both samples. No peak is observed at 180ºC indicating that no free metallic Lithium is detectable in either heating cycles.

The second analysis of the 25Li alloy was performed up to 340ºC to determine if a richer Li intermetallic, LiSn, with higher transformation temperature, was present in the samples. The Sn-25Li sample milled for 12h indicated the presence of a phase transformation above the Sn melting temperature. However, the LiSn presence could not be confirmed on the analysed samples as no significant heat flow perturbation was observed at the LiSn peritectic decomposition temperature, ~326ºC. Also, contrarily to the 1st analysis performed for the sample milled for 12h using the 50ºC – 250ºC temperature interval, for the first heating cycle the observed eutectic decomposition peak is much stronger than the remaining peaks, indicating that the eutectic mixture is the major constituent present in the tested sample. On the 2nd heating run, this sample also shows a different tendency than the remaining samples. It's the only sample where an increase of the eutectic peak heat flow was detected. As the samples tested using different temperature ranges were taken from the same batch, the detected differences in the results are attributed to inhomogeneity of the samples coupled with limitations in the protocol used to test the samples, namely the sampling method and the small size of the samples (<6mg).

The DSC analysis for both the Sn-15Li and Sn-5Li alloys was carried out in the 50ºC – 250ºC temperature interval. The analysis indicates that two endothermic transformations occur in both alloys during the 1st heating cycle: the eutectic decomposition and pure Sn melting. On the DSC analysis of the Sn-15Li alloy 12h milled sample there is an overlap of three peaks in the temperature range between 220-235ºC. The 1st peak with onset at 220ºC is attributed to the eutectic transformation, the 2nd peak with onset around 223ºC may be attributed to the dissolution of Li_2Sn_5 above the eutectic temperature into the liquid and the 3rd peak is associated with melting of free β-Sn.

During the 2nd heating both the 5Li- and Sn-15Li alloy samples show a similar behaviour to the Sn-25Li alloy: a non-reversible phase transformation occurs after the 1st heating inducing a general decrease of the eutectic peak and an increase of the Sn melting peak upon the 2nd heating.

The overlap of several peaks during cooling was observed in both the DSC cooling curves of all alloys. When pure Li and pure Sn samples were tested, the

solidification exothermic peaks are well defined. However, when Li and Sn are alloyed together, several overlapping peaks (over 20 in some cases) were detected. The peaks cannot be assigned to any solidification or transformation event described in the phase diagram (Figure 2). Results show that when the concentration of Li increases, the occurrence of these peaks occurs at lower temperatures. The cause for the appearance of this peaks could not be determined in this work but may be attributed to the segregation of Li towards the surface observed when Sn-Li alloys melt [21]–[24]. As this segregation proceeds, the surface layers of the melt become richer in Li than the bulk of the liquid. As Li content increases in some areas, the local equilibrium shifts towards the Li rich side of the phase diagram. The peaks detected may be attributed to the formation of higher Li concentration intermetallic compounds which do not melt within the DSC tested temperatures. This segregation may be the mechanism behind the apparent increase in the free β-Sn peak observed on the 2nd heating run of most samples: as the surface layers enrich with Li, the bottom layers become depleted of Li, increasing the amount of free β-Sn. At room temperature, solid Li vapour pressure is very low (10^{-22} atm). At the temperatures analysed with DSC, Li can reach a vapour pressure of 5,99 x 10^{-11} atm at 250ºC and of 1,29 x 10^{-8} atm at 340ºC [25]. Studies have also shown that Sn-Li alloys show lower evaporation rates than pure Li [1]. Thus Li evaporation rate should always be small within the tested conditions and so Li losses by evaporation negligible. Li evaporation cannot support the identified changes between the 1st and 2nd DSC thermal cycles.

5. Conclusions

Several experiments were conducted to determine the feasibility of producing Sn-Li alloys with Li compositions in the 25 - 5 Li at% interval by mechanical alloying. The production of Sn-Li alloys was successful, with three compositions being manufactured: 25, 15 and 5 at% Li. Small deviations from the designed compositions were observed. These deviations are attributed to the inhomogeneity of the samples demonstrated both with IBA and DSC.

The milling process overall yield seems to be limited by the energy input: increase in energy results in more losses of material to the walls due to adhesion of massive cold-welded material. The maximum milling time tested in this work was 24h due to limitation induced by the adhesion of cold-welded milled material to the vial walls.

The powders start as irregular, rugose powders, that evolve to become more faceted as the milling time increases. Increasing the Li content increases the rugosity of the powders for the same milling times and decreasing the Li content decreases the time needed to achieve faceted or spherical, smooth powders.

The overall results allow concluding that the process produced metastable microstructures with metallic Sn being present even in hypereutectic compositions. It was not possible to determine if higher melting point intermetallic compounds formed during reactive milling of Li with Sn. Further testing is necessary to determine the distribution of phases which can be achieved either by improving the milling process to allow the production of more representative samples or using devices that allow constant manipulation of the samples under protective argon atmosphere.

6. Acknowledgements

The author acknowledge Makin Metal Powders (UK) Ltd for supplying the Sn powder and Foundation for Science and Technology (FCT, Portugal) for financial support under project UID/CTM/04540/2013 (CeFEMA).

7. References

[1] R. E. Nygren and F. L. Tabarés, “Liquid surfaces for fusion plasma facing components—A critical review. Part I: Physics and PSI,” *Nucl. Mater. Energy*, vol. 9, pp. 6–21, 2016.

[2] K. Natesan and W. E. Ruther, “Fabrication and properties of a tin-lithium alloy,” *J. Nucl. Mater.*, vol. 307–311, no. 1 SUPPL., pp. 743–748, 2002.

[3] Y. Nakajima, M. Kondo, and T. Nozawa, “Study on fabrication method of lithium alloys with metal grains,” *Fusion Eng. Des.*, vol. 98–99, pp. 2009–2014, 2015.

[4] C. Suryanarayana and N. Al-Aqeeli, “Mechanically alloyed nanocomposites,” *Prog. Mater. Sci.*, vol. 58, no. 4, pp. 383–502, 2013.

[5] J. W. Coenen *et al.*, “Liquid metals as alternative solution for the power exhaust of future fusion devices: status and perspective,” *Phys. Scr.*, vol. 2014, no. T159, p. 14037, 2014.

[6] Y. Nagayama, “Liquid lithium divertor system for fusion reactor,” *Fusion Eng. Des.*, vol. 84, no. 7, pp. 1380–1383, 2009.

[7] J. P. S. Loureiro *et al.*, “Behavior of liquid Sn-Li alloy as plasma facing material on ISTTOK,” *Fusion Eng. Des.*, vol. 117, pp. 208–211, 2017.

[8] J. P. Allain, D. N. Ruzic, and M. R. Hendricks, “D, He and Li sputtering of liquid eutectic Sn-Li,” *J. Nucl. Mater.*, vol. 290–293, pp. 33–37, 2001.

[9] F. L. Tabarés, “Present status of liquid metal research for a fusion reactor,” *Plasma Phys. Control. Fusion*, vol. 58, no. 1, 2015.

[10] F. Robert *et al.*, “Mechanosynthesis and characterisation of the Sn-Li system,” *Hyperfine Interact.*, vol. 167, no. 1–3, pp. 797–801, 2006.
[11] F. Robert *et al.*, “Mössbauer spectra as a ‘fingerprint’ in tin-lithium compounds: Applications to Li-ion batteries,” *J. Solid State Chem.*, vol. 180, no. 1, pp. 339–348, 2007.
[12] K. N. Ishihara, F. Kubo, E. Yamasue, and H. Okumura, “Formation of supersaturated Fe-Li solid solution by mechanical alloying,” *Rev. Adv. Mater. Sci.*, vol. 18, no. 3, pp. 284–288, 2008.
[13] K. N. Ishihara, K. Irie, F. Kubo, E. Yamasue, and H. Okumura, “Mechanical milling of Fe-Li and Cu-Li systems and their nitrogen absorption properties,” *Mater. Sci. Eng. A*, vol. 448–451, pp. 1067–1070, 2007.
[14] K. N. Ishihara, F. Kubo, K. Irie, K. Shichi, E. Yamasue, and H. Okumura, “Mechanical alloying of lithium-base systems,” *J. Alloys Compd.*, vol. 434–435, no. SPEC. ISS., pp. 542–545, 2007.
[15] J. Shi, W. Shi, W. Jin, and G. Yin, “Diffusion of lithium in alpha-Sn and beat-Sn as anode materials for lithium ion batteries,” *Int. J. Electrochem. Sci.*, vol. 10, no. 6, pp. 4793–4800, 2015.
[16] C.-H. Chen, E. Chason, and P. R. Guduru, “Numerical Solution of Moving Phase Boundary and Diffusion-Induced Stress of Sn Anode in the Lithium-Ion Battery,” *J. Electrochem. Soc.*, vol. 164, no. 11, pp. E3661–E3670, 2017.
[17] P. Zhang, Z. Ma, W. Jiang, Y. Wang, Y. Pan, and C. Lu, “Mechanical properties of Sn-Li alloys for Li-ion battery anodes: A first-principles perspective,” *AIP Adv.*, vol. 6, no. 1, 2016.
[18] L. Vitos, A. V. Ruban, H. L. Skriver, and J. Kollár, “The surface energy of metals,” *Surf. Sci.*, vol. 411, no. 1–2, pp. 186–202, 1998.
[19] *Predel B. () Sn-Li (Lithium-Tin). In: Madelung O. (eds) Li-Mg – Nd-Zr. Landolt-Börnstein - Group IV Physical Chemistry (Numerical Data and Functional Relationships in Science and Technology), vol 5H. Springer, Berlin, Heidelberge. .*
[20] F. Grønvold, “Enthalpy of fusion and temperature of fusion of indium, and redetermination of the enthalpy of fusion of tin,” *J. Chem. Thermodyn.*, vol. 25, no. 9, pp. 1133–1144, 1993.
[21] H. Search, C. Journals, A. Contact, and M. Iopscience, “Structure of liquid Sn-Li alloys,” vol. 1995, 1995.
[22] M. A. Fütterer *et al.*, “On the use of tin-lithium alloys as breeder material for blankets of fusion power plants,” *J. Nucl. Mater.*, vol. 283–287, no. Part 2, pp. 1375–1379, 2000.
[23] R. Bastasz and W. Eckstein, “Plasma-surface interactions on liquids,” *J. Nucl. Mater.*, vol. 290–293, pp. 19–24, 2001.
[24] R. Bastasz and J. A. Whaley, “Surface composition of liquid metals and alloys,” *Fusion Eng. Des.*, vol. 72, no. 1–3 SPEC. ISS., pp. 111–119, 2004.
[25] C. B. Alcock, V. P. Itkin, and M. K. Horrigan, “Vapor Pressure of the Metallic Elements,” *Can. Metall. Q.*, vol. 23, no. 3, pp. 309–313, 1984.
[26] “Predel B. () Li-W (Lithium-Tungsten). In: Madelung O. (eds) Li-Mg – Nd-Zr. Landolt-Börnstein - Group IV Physical Chemistry (Numerical Data and Functional Relationships in Science and Technology), vol 5H. Springer, Berlin, Heidelberg.”